



Neural network
volcanic ash
detection

T. M. Gray and
R. Bennartz

This discussion paper is/has been under review for the journal Atmospheric Measurement Techniques (AMT). Please refer to the corresponding final paper in AMT if available.

Automatic volcanic ash detection from MODIS observations using a back-propagation neural network

T. M. Gray and R. Bennartz

Department of Earth and Environmental Sciences, Vanderbilt University, Nashville, Tennessee, USA

Received: 12 June 2015 – Accepted: 21 July 2015 – Published: 19 August 2015

Correspondence to: R. Bennartz (ralf.bennartz@vanderbilt.edu)

Published by Copernicus Publications on behalf of the European Geosciences Union.

Title Page

Abstract

Introduction

Conclusions

References

Tables

Figures



Back

Close

Full Screen / Esc

Printer-friendly Version

Interactive Discussion



Abstract

Due to the climate effects and aviation threats of volcanic eruptions, it is important to accurately locate ash in the atmosphere. This study aims to explore the accuracy and reliability of training a neural network to identify cases of ash using observations from the Moderate Resolution Imaging Spectroradiometer (MODIS). Satellite images were obtained for the following eruptions: Kasatochi, Aleutian Islands, 2008; Okmok, Aleutian Islands, 2008; Grímsvötn, northeastern Iceland, 2011; Chaiteín, southern Chile, 2008; Puyehue-Cordón Caulle, central Chile, 2011; Sangeang Api, Indonesia, 2014; and Kelut, Indonesia, 2014. The Hybrid Single Particle Lagrangian Integrated Trajectory Model (HYSPLIT) was used to obtain ash concentrations for the same archived eruptions. Two back-propagation neural networks were then trained using brightness temperature differences as inputs obtained via the following band combinations: 12-11, 11-8.6, 11-7.3, and 11 μm . Using the ash concentrations determined via HYSPLIT, flags were created to differentiate between ash (1) and no ash (0) and SO₂-rich ash (1) and no SO₂-rich ash (0) and used as output. When neural network output was compared to the test dataset, 93 % of pixels containing ash were correctly identified and 7 % were missed. Nearly 100 % of pixels containing SO₂-rich ash were correctly identified. The optimal thresholds, determined using Heidke skill scores, for ash retrieval and SO₂-rich ash retrieval were 0.48 and 0.47, respectively. The networks show significantly less accuracy in the presence of high water vapor, liquid water, ice, or dust concentrations. Significant errors are also observed at the edge of the MODIS swath.

1 Introduction

Volcanic eruptions, if large enough, can have a dramatic effect on the climate and the aviation industry, as highly explosive eruptions can emit large amounts of ash and SO₂ into the troposphere and stratosphere. Due to climate and aviation impacts, the knowledge of the location of volcanic ash following an eruption is imperative. Although

AMTD

8, 8753–8777, 2015

Neural network volcanic ash detection

T. M. Gray and
R. Bennartz

Title Page

Abstract

Introduction

Conclusions

References

Tables

Figures



Back

Close

Full Screen / Esc

Printer-friendly Version

Interactive Discussion



compared. More information about these specific eruptions can be found in Appendix A. The focus of this paper will be on four of the seven eruptions: Chaitein, Okmok, Kelut, and Sangeang Api. Additional information regarding the other three eruptions has been provided as Supplement.

2.2 Remote sensing

Aerosols exhibit varying transmittance in the 8–10 and 10–12 μm ranges, regions where the atmosphere is nearly transparent (Ackerman, 1997). Because MODIS channels 29, 31, and 32 cover this spectral range, MODIS images were obtained and band combinations were applied to determine areas of ash and SO_2 in each eruptive column. Sulfur dioxide is very absorptive in 7.3 and 8.6 μm channels (Prata et al., 2007). However, the 7.3 μm channel is not as sensitive to the total SO_2 column as the 8.6 μm channel because the 7.3 μm channel lies within a band that is also sensitive to water vapor (Sears et al., 2013) (see Fig. 1 in Watson et al., 2004). Band differencing was used to locate both ash and SO_2 in the atmosphere following a volcanic eruption. Ash is characterized by a negative brightness temperature difference between 11 and 12 μm (Ackerman et al., 2008). Ice is characterized by a positive brightness temperature difference between 11 and 12 μm because ice exhibits a lower brightness temperature at 12 μm (Watson et al., 2004). Following methods similar to Ackerman et al. (2008), band 31 (11 μm) was subtracted from band 32 (12 μm) to create a positive brightness temperature difference representing ash. Because SO_2 absorbs strongly in the 8.6 μm channel but not in the 11 μm channel, band 29 (8.6 μm) was subtracted from band 31 (11 μm) to create a positive brightness temperature difference representing SO_2 (Figs. 1–4). Visible images were also created for each case by combining band 1 (620–670 nm), band 4 (545–565 nm), and band 3 (459–479 nm) (Figs. 1–4).

Neural network volcanic ash detection

T. M. Gray and
R. Bennartz

Title Page

Abstract

Introduction

Conclusions

References

Tables

Figures

◀

▶

◀

▶

Back

Close

Full Screen / Esc

Printer-friendly Version

Interactive Discussion



2.3 HYSPLIT

After band combinations were used to differentiate between ambient clouds, surface features, ash, and SO₂, ash concentrations were determined using the Hybrid Single-Particle Lagrangian Integrated Trajectory (HYSPLIT) Model for Volcanic Ash for the same archived eruptions (Draxler and Rolph, 2003).

The NOAA/Air Resources Laboratory HYSPLIT model can be used specifically for archived volcanic eruptions to determine the transport, dispersion, and ash concentrations of the volcanic plume. For this particular study, National Centers for Environmental Prediction (NCEP)/National Center for Atmospheric Research (NCAR) Reanalysis meteorological data was used. Reanalysis data is composed of atmospheric analysis reproduced using historical data (1948-current) (Kalnay et al., 1996). These concentrations were then used to create “ash” and “no-ash” classifications, which may or may not be representative of reality due to HYSPLIT concentration uncertainties. Parameters specified in this model can be found in Appendix B. Concentrations were integrated over the concentration layer height of 30 or 32 km, depending on the eruption, resulting in units of g m⁻².

2.4 Neural network

A neural network, or a structure that mathematically identifies relationships between given inputs and outputs (Hsu et al., 1995), is made up of neurons, which consist of input signals, a set of weights, activation levels, and threshold functions (Luger and Stubblefield, 1998). Neural networks have varying topologies, learning algorithms, and encoding schemes (Luger and Stubblefield, 1998). This particular study used a back-propagation learning algorithm for a multi-layer neural network, which propagates error backwards starting from the output layer through the hidden layers, which connect the input and output layers (Luger and Stubblefield, 1998).

Neural network volcanic ash detection

T. M. Gray and
R. Bennartz

Title Page

Abstract

Introduction

Conclusions

References

Tables

Figures



Back

Close

Full Screen / Esc

Printer-friendly Version

Interactive Discussion



2.4.1 Neural network training

Two back-propagation neural networks were used to determine whether or not ash or SO₂-rich ash was present in a given MODIS pixel. From 120 MODIS granules, 14 cases were chosen where HYSPLIT output was well aligned with satellite observations (Appendix B). Three masks were applied to each granule to create a selection of pixels containing only ash, a selection containing only SO₂-rich ash, and a selection containing all other situations where ash was not present. Both networks were trained using inputs obtained via the following band combinations: 12-11 μm brightness temperature difference, 11-8.6 μm brightness temperature difference, 11-7.3 μm brightness temperature difference, and 11 μm brightness temperature. Using the ash concentrations determined via HYSPLIT, two sets of flags were created to differentiate between ash (1) and no ash (0), and SO₂-rich ash (1) and no SO₂-rich ash (0). As validation, the neural networks used these flag as outputs. The back-propagation neural network settings used in this study can be found in the Supplement. Dr. René Preusker, Institute for Space Sciences, Free University of Berlin, Germany, created the software used in this study for the training of this particular neural network.

3 Results

3.1 Optimal thresholds

The neural network output was compared to the test dataset output for both the ash-detection and SO₂-rich-ash-detection networks. A Heidke skill score (HSS) was calculated for all possible ash/no ash and SO₂-rich ash/no SO₂-rich ash thresholds to determine optimal thresholds (Fig. 5 and 6). Data used to make these plots has been provided.

The optimal thresholds for ash retrieval and SO₂-rich ash retrieval were 0.48 and 0.47, respectively. The SO₂-rich-ash-detection neural network was found to have

Neural network volcanic ash detection

T. M. Gray and
R. Bennartz

Title Page

Abstract

Introduction

Conclusions

References

Tables

Figures



Back

Close

Full Screen / Esc

Printer-friendly Version

Interactive Discussion



Neural network volcanic ash detection

T. M. Gray and
R. Bennartz

Title Page

Abstract

Introduction

Conclusions

References

Tables

Figures

◀

▶

◀

▶

Back

Close

Full Screen / Esc

Printer-friendly Version

Interactive Discussion



In order to train the network, HYSPLIT was treated to be representative of reality. This may not always be accurate, especially for eruptions characterized by multiple eruptive pulses. One of the limitations of HYSPLIT is that it can only be used with one eruptive pulse or one continuous ash release. Chaitén, which was characterized by two significant eruptive pulses four days apart, was one case where HYSPLIT and MODIS were not well aligned. The second pulse was analyzed in this study, but low-level ash was still present in the atmosphere from the previous eruption. HYSPLIT had no way of knowing this, which could lead to missed ash within the training of the neural network. Another limitation of this study is the lack of knowledge about erupted ash quantity from some events. When unknown, USGS parameters were used, which could lead to significant errors within HYSPLIT and thus the training of the neural network.

The location of volcanic ash in the atmosphere is crucial information for the aviation industry, as volcanic ash can heavily damage jet engines and other parts of aircraft, as discussed in Sect. 2.6. This particular study can be used to automatically detect ash in MODIS observations, providing critical information to the aviation industry. However, this study does not yet provide information about the concentration of ash in each pixel or the altitude of the ash. Currently, this study only provides confirmation of the presence of ash and/or SO₂-rich ash within a 30 km vertical column.

Future work will include determining the accuracy of training an additional neural network to detect not only whether or not ash is present, but also ash concentration and ash cloud altitude.

Appendix: Volcanoes

Located in the Aleutian Islands, the basaltic shield volcano Okmok, erupted at 19:43 UTC on 12 July 2008 (Fee et al., 2010), with a plume height near 15 km (GVP). This phreatomagmatic eruption, or one characterized by high water content (Fee et al., 2010), released 0.1 Tg of SO₂ (Prata et al., 2010).

**Neural network
volcanic ash
detection**T. M. Gray and
R. Bennartz

Title Page

Abstract

Introduction

Conclusions

References

Tables

Figures



Back

Close

Full Screen / Esc

Printer-friendly Version

Interactive Discussion



Chaitén, a rhyolitic caldera in southern Chile, began erupting on 2 May 2008 (Lara, 2009). This eruptive event continued for months, but on 6 May 2008, 12:32 UTC, produced the second Plinian column of the event with a plume height of over 20 km (Lara, 2009; GVP). This eruption is especially interesting as it was the first rhyolitic eruption during the satellite era (Lara, 2009). This eruption was not associated with high SO₂ emissions (Lara, 2009; Carn et al., 2009b).

On 13 February 2014, 15:50 UTC, Kelut, a stratovolcano located in Java, began erupting. This eruption sent volcanic ash to altitudes of 17 km, continued for 3–4 days, and resulted in 40 canceled flights and multiple rerouted flights (GVP; Kristiansen et al., 2015). Kelut is estimated to have injected a total of 0.74 Tg of ash into the atmosphere, and 0.38 Tg of that ash into the stratosphere (Kristiansen et al., 2015).

Sangeang Api, a volcanic complex in the Lesser Sunda Islands (Sigurdsson, 2000), began erupting on 30 May 2014, 08:55 UTC (GVP). This trachybasaltic-to-trachyandesitic complex emitted ash up to 15.2 km and resulted in canceled flights from the Darwin International Airport (GVP).

**The Supplement related to this article is available online at
doi:10.5194/amtd-8-8753-2015-supplement.**

Acknowledgements. The authors would like to thank Mike Pavolonis of NOAA for helpful scientific discussions. A special thanks also goes to John Rausch at Vanderbilt University for programming assistance. This work was supported by an internal Vanderbilt research grant to Ralf Bennartz.

References

Achterberg, E. P., Moore, C. M., Henson, S. A., Steigenberger, S., Stohl, A., Eckhardt, S., Avendano, L. C., Cassidy, M., Hembury, D., Klar, J. K., Lucas, M. I., Macey, A. I., Marsay, C. M., and Ryan-Keogh, T. J.: Natural iron fertilization by the Eyjafjallajökull volcanic eruption, *Geophys. Res. Lett.*, 40, 921–926, 2013.

Neural network volcanic ash detection

T. M. Gray and
R. Bennartz

Title Page

Abstract

Introduction

Conclusions

References

Tables

Figures



Back

Close

Full Screen / Esc

Printer-friendly Version

Interactive Discussion



- Ackerman, S. A.: Remote sensing aerosols using satellite infrared observations, *J. Geophys. Res.-Atmos.*, 102, 17069–17079, 1997.
- Ackerman, S. A., Schreiner, A. J., Schmit, T. J., Woolf, H. M., Li, J., and Pavolonis, M.: Using the GOES Sounder to monitor upper level SO₂ from volcanic eruptions, *J. Geophys. Res.*, 113, D14s11, doi:10.1029/2007jd009622, 2008.
- Albrecht, B. A.: Aerosols, cloud microphysics, and fractional cloudiness, *Science*, 245, 1227–1230, 1989.
- Caldeira, K. G., Rampino, M. R.: Deccan volcanism, greenhouse warming, and the Cretaceous/Tertiary boundary, *Geol. S. Am. S.*, 247, 117–124, 1990.
- Carn, S. A. and Prata, F. J.: Satellite-based constraints on explosive SO₂ release from Soufrière Hills Volcano, Montserrat, *Geophys. Res. Lett.*, 37, L00E22, doi:10.1029/2010GL044971, 2010.
- Carn, S. A., Schneider, D. J., Bluth, G. J., Kobs, S. E., Rose, W. I., and Ernst, G. G.: On the separation of ash and sulfur dioxide in volcanic clouds, AGU Spring Meeting Abstracts, Abstract V51A-03, Washington, DC, 28–31 May, 2002.
- Carn, S. A., Krueger, A. J., Krotkov, N. A., Yang, K., and Evans, K.: Tracking volcanic sulfur dioxide clouds for aviation hazard mitigation, *Nat. Hazards*, 51, 325–343, 2009a.
- Carn, S. A., Pallister, J. S., Lara, L., Ewert, J. W., Watt, S., Prata, A. J., Thomas, R. J., and Villarosa, G.: The Unexpected Awakening of Chaitén Volcano, Chile, *EOS T. Am. Geophys. Un.*, 90, 205–206, 2009b.
- Corradini, S., Merucci, L., Prata, A. J., and Piscini, A.: Volcanic ash and SO₂ in the 2008 Kasatochi eruption: retrievals comparison from different IR satellite sensors, *J. Geophys. Res.*, 115, D00L21, doi:10.1029/2009JD013634, 2010.
- Diaz, S. B., Paladini, A. A., Braile, H. G., Dieguez, M. C., Deferrari, G. A., Vernet, M., and Vrsalovic, J.: Global and direct UV irradiance variation in the Nahuel Huapi National Park (Patagonia, Argentina) after the eruption of Puyehue-Cordon Caulle (Chile), *J. Atmos. Sol.-Terr. Phy.*, 112, 47–56, 2014.
- Draxler, R. R. and Rolph, G. D.: HYSPLIT (Hybrid Single-Particle Lagrangian Integrated Trajectory) Model access via NOAA ARL READY Website, available at: <http://www.arl.noaa.gov/ready/hysplit4.html> (last access: 15 August 2015), NOAA Air Resources Laboratory, Silver Spring, MD, USA, 2003.

Neural network volcanic ash detection

T. M. Gray and
R. Bennartz

Title Page

Abstract

Introduction

Conclusions

References

Tables

Figures



Back

Close

Full Screen / Esc

Printer-friendly Version

Interactive Discussion



- Fee, D., Steffke, A., and Garces, M.: Characterization of the 2008 Kasatochi and Okmok eruptions using remote infrasound arrays, *J. Geophys. Res.*, 115, D00L10, doi:10.1029/2009JD013621, 2010.
- Feltz, W. F., Bedka, K., Wimmers, A. J., Pavolonis, M., Bedka, S. M., Ackerman, S.: Satellite-derived products to enhance aviation nowcasting of convection, turbulence, and volcanic ash, Paper presented at the 14th Conference on Satellite Meteorology and Oceanography, 27 January–3 February 2006, Atlanta, GA, 2006.
- Flanner, M. G., Gardner, A. S., Eckhardt, S., Stohl, A., and Perket, J.: Aerosol radiative forcing from the 2010 Eyjafjallajökull volcanic eruptions, *J. Geophys. Res.-Atmos.*, 119, 9481–9491, 2014.
- Francis, P. and Oppenheimer, C.: *Volcanoes*, Oxford UP, Oxford, 2004.
- Global Volcanism Program (GVP): <http://www.volcano.si.edu/>, last access: 15 April 2014.
- Hsu, K. L., Gupta, H. V., and Sorooshian, S.: Artificial neural-network modeling of the rainfall-runoff process, *Water. Resour. Res.*, 31, 2517–2530, 1995.
- ICAO (International Civil Aviation Organization): *Manual on Volcanic Ash, Radioactive Material, and Toxic Chemical Clouds*, 2nd edn., Doc 9691-AN/954, International Civil Aviation Organization, 999 University Street, Montréal, Quebec, Canada H3C 5H7, 2007.
- Kalnay, E., Kanamitsu, M., Kistler, R., Collins, W., Deaven, D., Gandin, L., Iredell, M., Saha, S., White, G., Woollen, J., Zhu, Y., Chelliah, M., Ebisuzaki, W., Higgins, W., Janowiak, J., Mo, K. C., Ropelewski, C., Wang, J., Leetmaa, A., Reynolds, R., Jenne, R., and Joseph, D.: The NCEP/NCAR 40-year reanalysis project, *B. Am. Meteorol. Soc.*, 77, 437–471, 1996.
- Klüser, L., Erbertseder, T., and Meyer-Arneke, J.: Observation of volcanic ash from Puyehue–Cordón Caulle with IASI, *Atmos. Meas. Tech.*, 6, 35–46, doi:10.5194/amt-6-35-2013, 2013.
- Kravitz, B. and Robock, A.: Climate effects of high-latitude volcanic eruptions: role of the time of year, *J. Geophys. Res.*, 116, D01105, doi:10.1029/2010JD014448, 2011.
- Kristiansen, N. I., Prata, A. J., Stohl, A., and Carn, S. A.: Stratospheric volcanic ash emissions from the 13 February 2014 Kelut eruption, *Geophys. Res. Lett.*, 42, 588–596, 2015.
- Langmann, B.: Volcanic ash versus mineral dust: atmospheric processing and environmental and climate impacts, *ISRN Atmospheric Sciences*, 2013, 1–17, 2013.
- Langmann, B.: On the role of climate forcing by volcanic sulphate and volcanic ash, *Advances in Meteorology*, 2014, 1–17, 2014.
- Lara, L. E.: The 2008 eruption of the Chaitén Volcano, Chile: a preliminary report, *Andean Geol.*, 36, 125–129, 2009.

Neural network volcanic ash detection

T. M. Gray and
R. Bennartz

Title Page

Abstract

Introduction

Conclusions

References

Tables

Figures



Back

Close

Full Screen / Esc

Printer-friendly Version

Interactive Discussion



Rose, W. I., Bluth, G. J. S., and Ernst, G. G. J.: Integrating retrievals of volcanic cloud characteristics from satellite remote sensors: a summary, *Philos. T. R. Soc A*, 358, 1585–1606, 2000.

Schneider, D. J., Rose, W. I., Coke, L. R., Bluth, G. J., Sprod, I. E., and Krueger, A. J.: Early evolution of a stratospheric volcanic eruption cloud as observed with TOMS and AVHRR, *J. Geophys. Res.-Atmos.*, 104, 4037–4050, 1999.

Sears, T. M., Thomas, G. E., Carboni, E., A. Smith, A. J., and Grainger, R. G.: SO₂ as a possible proxy for volcanic ash in aviation hazard avoidance, *J. Geophys. Res.-Atmos.*, 118, 5698–5709, 2013.

Sigurdsson, H.: *Encyclopedia of Volcanoes*, Academic Press, San Diego, CA, 2000.

Solomon, S., Daniel, J. S., Neely III, R. R., Vernier, J.-P., Dutton, E. G., and Thomason, L. W.: The persistently variable “background” stratospheric aerosol layer and global climate change, *Science*, 333, 866–870, 2011.

Theys, N., Campion, R., Clarisse, L., Brenot, H., van Gent, J., Dils, B., Corradini, S., Merucci, L., Coheur, P.-F., Van Roozendaal, M., Hurtmans, D., Clerbaux, C., Tait, S., and Ferrucci, F.: Volcanic SO₂ fluxes derived from satellite data: a survey using OMI, GOME-2, IASI and MODIS, *Atmos. Chem. Phys.*, 13, 5945–5968, doi:10.5194/acp-13-5945-2013, 2013.

Thomas, H. E. and Prata, A. J.: Sulphur dioxide as a volcanic ash proxy during the April–May 2010 eruption of Eyjafjallajökull Volcano, Iceland, *Atmos. Chem. Phys.*, 11, 6871–6880, doi:10.5194/acp-11-6871-2011, 2011.

Twomey, S.: Influence of pollution on shortwave albedo of clouds, *J. Atmos. Sci.*, 34, 1149–1152, 1977.

Vernier, J. P., Thomason, L. W., Pommereau, J. P., Bourassa, A., Pelon, J., Garnier, A., Hauchecorne, A., Blanot, L., Trepte, C., Degenstein, D., and Vargas, F.: Major influence of tropical volcanic eruptions on the stratospheric aerosol layer during the last decade, *Geophys. Res. Lett.*, 38, L12807, doi:10.1029/2011GL047563, 2011.

Watson, I. M., Realmuto, V. J., Rose, W. I., Prata, A. J., Bluth, G. J. S., Gu, Y., Bader, C. E., and Yu, T.: Thermal infrared remote sensing of volcanic emissions using the moderate resolution imaging spectroradiometer, *J. Volcanol. Geoth. Res.*, 135, 75–89, 2004.

Neural network volcanic ash detection

T. M. Gray and
R. Bennartz

Title Page

Abstract

Introduction

Conclusions

References

Tables

Figures



Back

Close

Full Screen / Esc

Printer-friendly Version

Interactive Discussion



Table 1. Seven volcanic eruptions and their corresponding time, location, plume height (km) and explosivity.

Volcano	Date of Eruption	Location	Plume Height (km)	VEI
Kasatochi	7 Aug 2008	52.177° N, 175.508° W	~ 19	4
Okmok	12 Jul 2008	53.43° N, 168.13° W	~ 15	4
Grímsvötn	21 May 2011	64.42° N, 17.33° W	~ 20	4
Chaitén	6 May 2008	42.833° S, 72.646° W	~ 30	4
Puyehue-Cordón Caulle	4 Jun 2011	40.59° S, 72.117° W	~ 12	3
Kelut	13 Apr 2014	7.93° S, 112.31° E	~ 17	4
Sangeang Api	30 May 2014	8.20° S, 119.07° E	~ 15	3

Neural network volcanic ash detection

T. M. Gray and
R. Bennartz

Title Page

Abstract

Introduction

Conclusions

References

Tables

Figures



Back

Close

Full Screen / Esc

Printer-friendly Version

Interactive Discussion



Table 2. (Top) Ash-detection neural network output was compared to the test dataset output to measure success; (Bottom) SO₂-rich-ash-detection neural network output was compared to the test dataset to measure success.

Ash Observed	Ash Predicted	
	No	Yes
No	87.7 %	12.3 %
Yes	6.8 %	93.2 %
SO ₂ -rich Ash Observed	SO ₂ -rich Ash Predicted	
	No	Yes
No	98.4 %	1.6 %
Yes	0.03 %	99.97 %

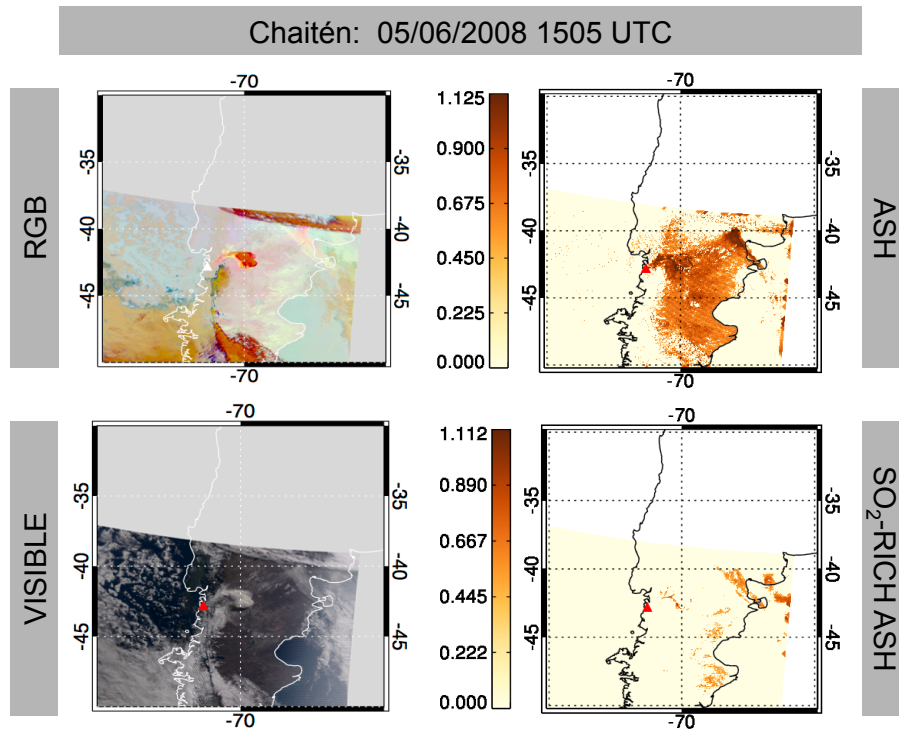


Figure 1. (Top left) RGB created using MODIS bands 32-31, 31-29, and 31 for the eruption of Chaitén, 6 May 2008, 1505Z; (bottom left) visible image created using MODIS bands 1, 4, and 3 for the same eruption and time; (top right) ash-detection neural network output for the same eruption and time; (bottom right) SO_2 -rich-ash-detection neural network output for the same eruption and time.

Neural network volcanic ash detection

T. M. Gray and
R. Bennartz

Title Page

Abstract

Introduction

Conclusions

References

Tables

Figures



Back

Close

Full Screen / Esc

Printer-friendly Version

Interactive Discussion



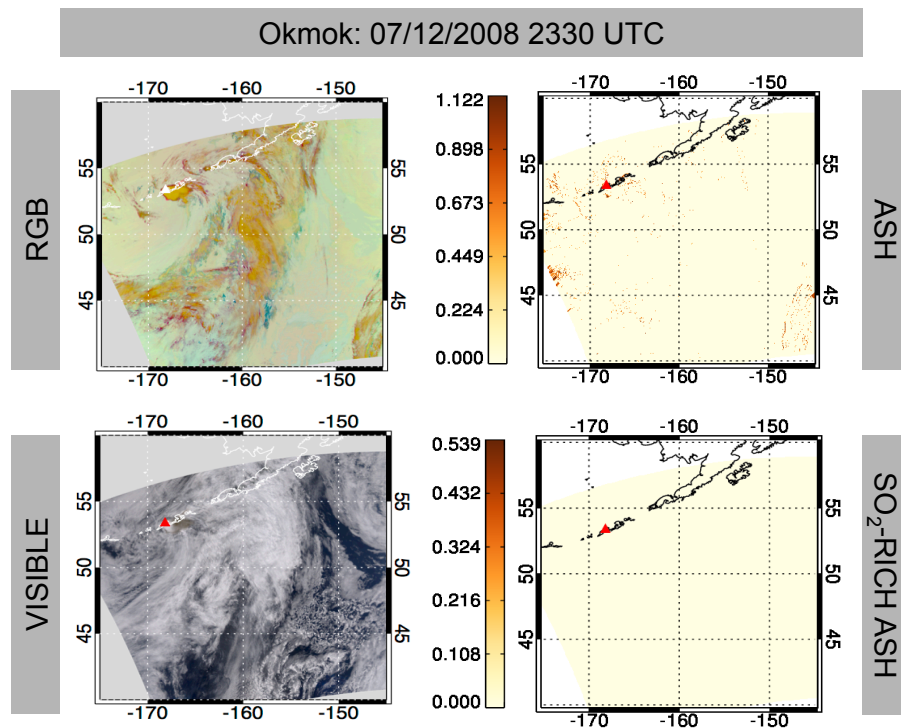


Figure 2. (Top left) RGB created using MODIS bands 32-31, 31-29, and 31 for the eruption of Okmok, 12 July 2008, 2330Z; (bottom left) visible image created using MODIS bands 1, 4, and 3 for the same eruption and time; (top right) ash-detection neural network output for the same eruption and time; (bottom right) SO₂-rich-ash-detection neural network output for the same eruption and time.

Neural network volcanic ash detection

T. M. Gray and
R. Bennartz

Title Page

Abstract

Introduction

Conclusions

References

Tables

Figures



Back

Close

Full Screen / Esc

Printer-friendly Version

Interactive Discussion



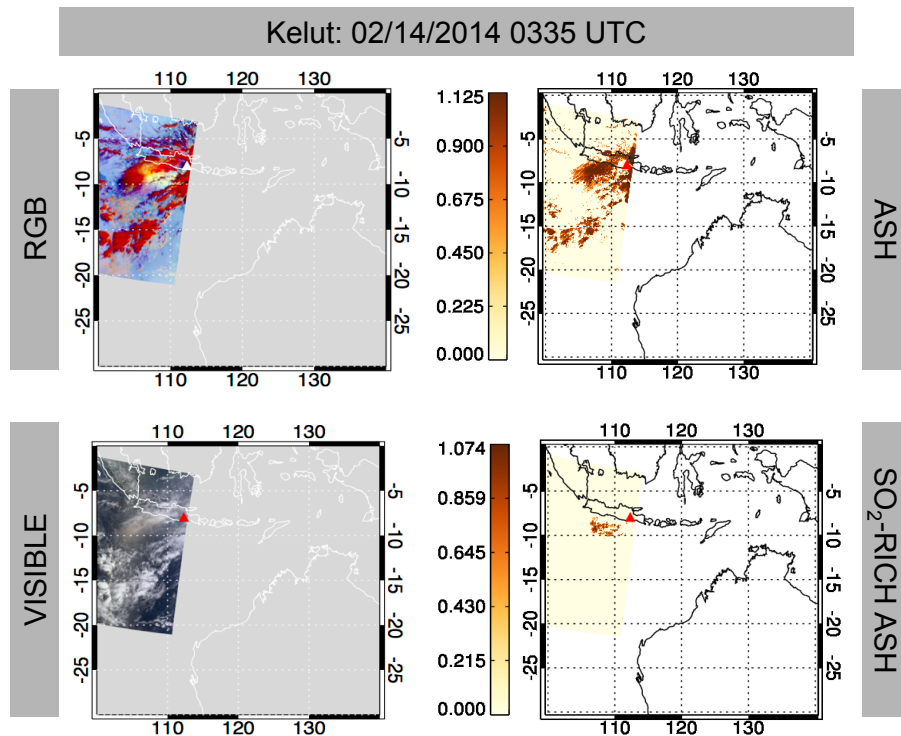


Figure 3. (Top left) RGB created using MODIS bands 32–31, 31–29, and 31 for the eruption of Kelut, 14 February, 0335Z; (bottom left) visible image created using MODIS bands 1, 4, and 3 for the same eruption and time; (top right) ash-detection neural network output for the same eruption and time; (bottom right) SO₂-rich-ash-detection neural network output for the same eruption and time.

Neural network volcanic ash detection

T. M. Gray and
R. Bennartz

Title Page

Abstract

Introduction

Conclusions

References

Tables

Figures

◀

▶

◀

▶

Back

Close

Full Screen / Esc

Printer-friendly Version

Interactive Discussion



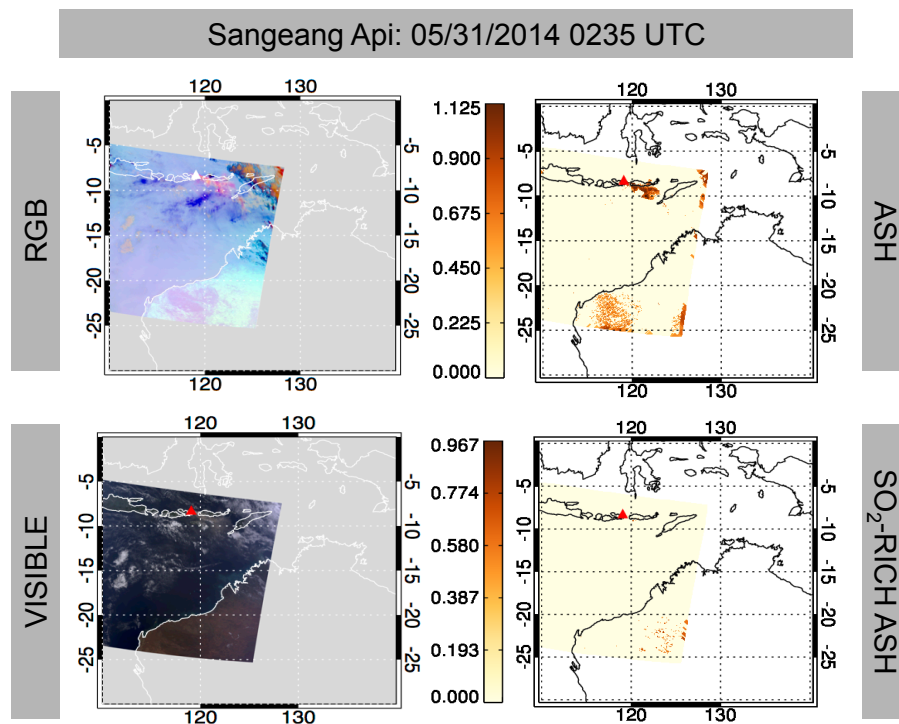


Figure 4. (Top left) RGB created using MODIS bands 32–31, 31–29, and 31 for the eruption of Sangeang Api, 31 May 2014, 0235Z; (bottom left) visible image created using MODIS bands 1, 4, and 3 for the same eruption and time; (top right) ash-detection neural network output for the same eruption and time; (bottom right) SO₂-rich-ash-detection neural network output for the same eruption and time.

Neural network volcanic ash detection

T. M. Gray and
R. Bennartz

Title Page

Abstract

Introduction

Conclusions

References

Tables

Figures



Back

Close

Full Screen / Esc

Printer-friendly Version

Interactive Discussion



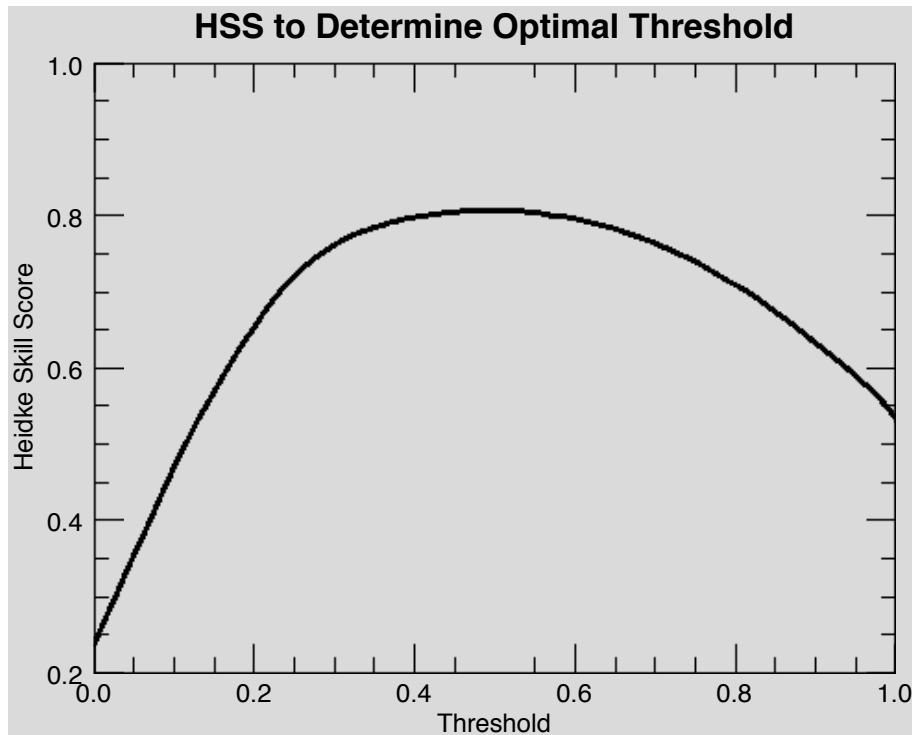


Figure 5. Optimal threshold for ash retrieval determined to be 0.48 with Heidke skill score of 0.81.

Neural network volcanic ash detection

T. M. Gray and
R. Bennartz

Title Page

Abstract

Introduction

Conclusions

References

Tables

Figures

◀

▶

◀

▶

Back

Close

Full Screen / Esc

Printer-friendly Version

Interactive Discussion



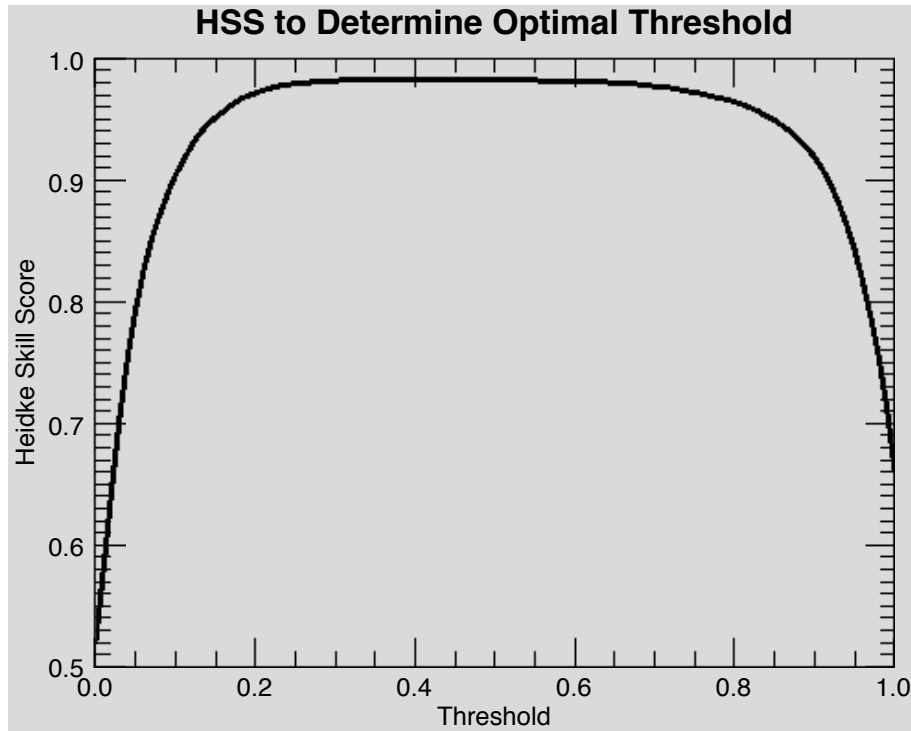


Figure 6. Optimal threshold for SO₂-rich ash retrieval determined to be 0.47 with Heidke skill score of 0.98.

Neural network volcanic ash detection

T. M. Gray and
R. Bennartz

Title Page

Abstract

Introduction

Conclusions

References

Tables

Figures

◀

▶

◀

▶

Back

Close

Full Screen / Esc

Printer-friendly Version

Interactive Discussion

